Surface reactivity and silanization ability of borosilicate and Mg-Sr-based bioactive glasses

Surface reactivity and silanization ability of borosilicate and Mg-Sr-based bioactive glasses

S. Ferraris [1], A. Nommeots-Nomm [2], S. Spriano [1], E. Vernè [1], J. Massera [2]

[1] Politecnico di Torino, Department of Applied Science and Technology, Institute of Materials Physics and Engineering, Torino, Italy;

[2] Tampere University of Technology, BioMediTech Institute and Faculty of Biomedical Sciences and Engineering, Tampere, Finland;

Corresponding author

Sara Ferraris

e-mail: sara.ferraris@polito.it

Phone: 0039-0110905768

Fax: 0039-0110904624

Abstract

Borosilicate bioactive glasses are attracting an increasing interest due to their good hot forming ability, low crystallization tendency and high bioactivity. Surface functionalization of bioactive glasses is a versatile tool for modulation of their properties and consequently of their biological response and it is still an unexplored topic in the case of borosilicate glasses. The possibility to graft 3-aminopropyltriethoxysilane (APTES) to various borosilicate bioactive glasses have been investigated in the present research work. Glasses were produced by melting and completely characterized (SEM-EDS, density, FTIR-ATR, Raman, NMR, zeta potential and reactivity in SBF and TRIS/HCl). Then, APTES was grafted to the surface of the glasses and its presence was verified by means of XPS, contact angle and zeta potential measurements. This study has shown the possibility to silanize borosilicate bioactive glasses for the first time, however, this silanization protocol does not induce the formation of a continuous coating on the glass surface.

Keywords: borosilicate bioactive glasses; silanization, APTES

1 Introduction

While surface functionalization of metals, polymers and ceramics has been widely studied in the past, functionalization of bioactive glasses has remained under investigated [1]. However, surface functionalization of bioactive glasses is a strategy that can produce materials with properties not attainable otherwise. Taken as an example, grafting biomolecules or drugs at the surface of bioactive glasses or glass-ceramic can lead to materials with enhanced therapeutic effect, cell stimulating ability or superior antimicrobial properties.

While surface modification and functionalization was developed in the past for pure silica glass a need for new protocols for the cleaning and silanization of reactive materials were needed. A protocol was developed by Vernè et al. [2, 3] for the exposition of hydroxyl groups onto silica based bioactive glasses. Post exposition of the hydroxyl groups, the surface was silanized using APTES. This molecule is widely used for surface modification of bioactive glasses and it can be considered both a model molecule to be grafted as well as a suitable spacer molecule for further grafting of bioactive moieties [4, 5]. The developed

technique has revealed to be promising toward a more efficient grafting of model protein such as Carnosine [2]. Verné el al. successfully grafted alkaline phosphatase at the surface of silanized silicate bioactive glass and improved both glass bioactivity and ability to stimulate osteoblasts cells [3]. Later, they proved that polyphenols extracted from grape skin could be immobilized at the surface of bioactive glasses [6]. This opens the path to the processing of smart biomaterials combining the known activity of bioactive glasses and the specific biological properties of natural molecules, i.e. antioxidant, antibacterial, antiviral, anticancer. This protocol was further adapted to phosphate bioactive glasses [7]. Recently, the authors also demonstrated that, careful surface washing and silanization of phosphate bioactive glass, can promote superior adsorption of albumin and fibronectin: these results will be published shortly thereafter.

Recently a new class of bioactive glasses has emerged, drawing increasing attention: borosilicate bioactive glasses. Borosilicate glasses have the advantage over their silicate counterpart to have better hot forming ability and lower crystallization tendency, making this glass family attractive toward the manufacturing of amorphous bioactive scaffolds or fibers [8, 9]. Furthermore, the borosilicate glasses show higher conversion rate to hydroxyapatite than pure silicate glasses [10].

In this context, the well-known bioactive glass S53P4 (called B0 in the present work, as starting point for the following compositional modifications), was modified by partial to fully substituting silica with boron. The structure of the glasses was studied via FTIR-ATR, Raman and ^{11}B NMR. Dissolution of the bioactive glass, with respect to the boron content was studied in Simulated Body Fluid (SBF). The release of ions was quantified using ICP-OES and the formation of a hydroxyapatite layer was confirmed by FTIR-ATR. Successively, Ca in the borosilicate glass was replaced by Sr and/or Mg and the dissolution study was repeated. Silanization of the glasses of investigation was conducted using the protocol developed in [2] and [7]. The effective silanization was further confirmed by XPS analysis, contact angle and Zeta-potential measurements.

2 Materials and methods

2.1 Glass synthesis

Glass B0 (S53P4) was melted from batches containing mixtures of silica (99.4 % pure SiO_2), and analytical grades of Na_2CO_3, H_3BO_3, $CaCO_3$, and $CaHPO_4.2H_2O$. The nominal oxide compositions of the experimental glasses in mol% are $(53.85-x)SiO_2$-xB_2O_3-$22.66Na_2O$-$1.72P_2O_5$-$21.77CaO$ with *x* varying from 0 to 53.85. The glasses were coded as follow: x = 0 (B0), x = 13.46 (B25), x= 26.93 (B50), x = 40.39 (B75) and x = 53.85 (B100). The glasses were melted in air in a platinum crucible at temperature from 1000 to 1400 ^oC for 3 h, depending on the boron content. The glass labelled B50 was also processed with various amount of magnesium and/or strontium substituted for calcium. The glass compositions investigated are presented in Table 1. After casting in a pre-heated cylindrical (Ø=10 mm) graphite mould, the glasses were annealed overnight at 40 ^oC below their respective glass transition temperature T_g and then allowed to cool slowly to room temperature in the annealing furnace. The obtained rods were either crushed into particles for the dissolution tests in simulated body fluid or sliced into discs (thickness 2 mm) ground and polished for surface functionalization.

Glass properties

SEM/EDX (Leo 1530 Gemini from Zeiss and EDXA UltraDry from Thermo Scientific) was used to image and analyse the samples composition. The accuracy of the elemental analysis is about 0.1 wt%.

The density of the bulk glass was measured by Archimedes' principle using deionized water. The accuracy was better than 0.02g/cm^3.

The IR absorption spectra of the glasses were recorded using Fourier transform infra-red spectroscopy (FTIR, Perkin Elmer) in attenuated total reflectance (ATR) mode on powdered glasses. All spectra were recorded within the range 650-1600 cm^{-1}, corrected for Fresnel losses and normalised to the absorption band showing the maximum intensity.

The Raman spectra were recorded using a 532 nm wavelength laser (Cobolt Samba) and measured with a 300 mm spectrograph (Andor Shamrock 303) and a cooled CCD camera for data collection (Andor

Newton 940P). All spectra were recorded within the range 500-1800 cm^{-1}, and normalised to the absorption band with the maximum intensity.

Solid State ^{11}B NMR experiments was carried out with a Bruker Avance 300 spectrometer working at 96 MHz for ^{11}B. The spectra were acquired under magic angle spinning (MAS) at a spinning rate of 14 kHz using a 4 mm diameter rotor. A simple pulse sequence was used and the probe signal was subtracted from the spectra acquired to ensure an easier reading. The ^{11}B chemical shift scales were calibrated with respect to B_2O_3 solutions. The spectra were reconstructed using the DMFIT software [11].

***In-vitro* dissolution test**

Glass particles between 125-250 μm were immersed in 50 ml of simulated body fluid (SBF) for 6, 24, 48, 72, and 168 h at 37 ^{o}C in an incubating shaker (INFORS Multitron II). An orbital speed of 100 RPM was chosen to give laminar flow mixing of the solution without inducing particle movement. The SBF was prepared using the protocol developed by Kokubo et al. [12]. The mass of the sample immersed in the solution was adjusted to maintain a constant surface area to volume ratio. The masses varied from 75 mg for the glass with x = 0 (B0) to 71.3 mg for the glass with x = 53.85 (B100) glass. For each time point four parallel samples of each glass were studied. The change in the solution pH was recorded for each immersion time and compared to a blank sample containing only SBF. After testing, the powder was washed with acetone and dried. Part of the powder was embedded in resin and polished to reveal the particulates' cross section. The composition and structure of the glass powder were analysed with SEM/EDX and FTIR-ATR.

Elemental concentrations in solution were measured using a Agilent technologies 5110 Inductively Coupled Plasma Optical Emission Spectrometer (ICP-OES) equipped with an auto sampler. Solutions were prepared by diluting the dissolution supernatant by a factor of 10 with distilled water and acidified with 69% nitric acid. Standards of the applicable elements; silicon, phosphorus, borate calcium, sodium, magnesium, and strontium were prepared at 0, 4, 10, 20 and 40 μg ml-1 to gain a calibration curve. Calibration was carried

out at the beginning of each sequence. Lines for analysis used: P: 253.561 nm, Sr: 216.596 nm, Mg: 279.553 nm, Si: 250.690 nm, Ca: 422.673 nm, B: 249.772 nm.

Table 1: Composition (in mol%) of selected borosilicate and Mg/Sr substituted glasses

			Borosilicate			**Mg/Sr substituted borosilicate**		
	B0	**B25**	**B50**	**B75**	**B100**	**B50Sr0**	**B50Sr5**	**B50Sr10**
SiO_2	53.86	40.40	26.93	13.47	0.00	26.93	26.93	26.93
B_2O_3	0.00	13.47	26.93	40.40	53.86	26.93	26.93	26.93
Na_2O	22.66	22.66	22.66	22.66	22.66	22.66	22.66	22.66
P_2O_5	1.72	1.72	1.72	1.72	1.72	1.72	1.72	1.72
CaO	21.77	21.77	21.77	21.77	21.77	16.77	11.77	6.77
MgO	0.00	0.00	0.00	0.00	0.00	5.00	5.00	5.00
SrO	0.00	0.00	0.00	0.00	0.00	0.00	5.00	10.00

2.5 Glass functionalization

In brief, samples were washed once in acetone (5 min in an ultrasonic bath) and subsequently three time in ultrapure water (5 min in an ultrasonic bath). For the surface functionalization 3-aminopropyltriethoxysilane (APTES) was chosen in order to introduce amino groups (-NH_2) on the glass surface.

For APTES grafting, samples were soaked 6 h at room temperature in 150 ml of ethanol containing 35 µl of 3-aminopropyltriethoxysilane (APTS, 99% Aldrich). At the end of the soaking period, the samples were extracted from the solution and thermally treated for 1h at 100°C in order to consolidate the silane-surface bonding. Samples were then washed three times in ethanol in an ultrasonic bath in order to remove unbounded molecules and then dried for 1 h at 100°C.

2.6 X-Ray Photoelectron Spectroscopy (XPS)

XPS (XPS, PHI 5000 VERSA PROBE, PHYSICAL ELECTRONICS) was employed for the surface characterization of bioactive glasses before and after silanization. Survey and high resolution spectra of carbon, oxygen and nitrogen regions were acquired in order to detect elements and functional groups at the surface before and after APTES grafting. The X-ray source was monochromatic Al K-alfa 1486 eV. Data were analyzed by multipak software (PHI electronics) and semiquantitative analysis was based on the relative sensitivity factors (RSF) library provided with multipak specifically for the PHI versa probe 5000.

2.7 Contact angle measurements

Sessile drop method was used to measure contact angle using ultrapure water as the wetting fluid. A drop of water (5 µl) was deposited upon the sample surface by means of a micro-tube. The image of the drop shape was acquired by a camera (Misura, Expert System Solutions) and the contact angle value was measured using Image J software (1.47 version).

2.8 Zeta potential measurements

An electrokinetic analyzer for solid surfaces (SurPASS, Anton Paar) was employed in order to measure the surface charge as a function of pH and the isoelectric point of pre and post silanized glasses by means of the streaming potential technique [13]. An adjustable gap cell was employed for the measurements. 0.001 M KCl was used as the electyrolyte and 0.05M HCl and 0.05M NaOH for the pH titration, performed by means of the instrument automatic titration unit. Because of the high surface reactivity of the studied materials two different couples of samples were considered in order to analyze the acid and the basic range of the test.

3. Results and discussion

3.1 Glass characterization

Figure 1 shows the density and molar volume of the glasses of investigation vs composition. With increasing the B_2O_3 substitution for SiO_2, the density of the glass decreased whereas the molar volume increased (Figure 1a). Similarly, while substitution of 5 mol% of CaO for MgO did not change the density of the glass, the addition of Sr leads to an increase. Within the accuracy of the measurement, the substitution of CaO with MgO and/or SrO did not impact the molar volume.

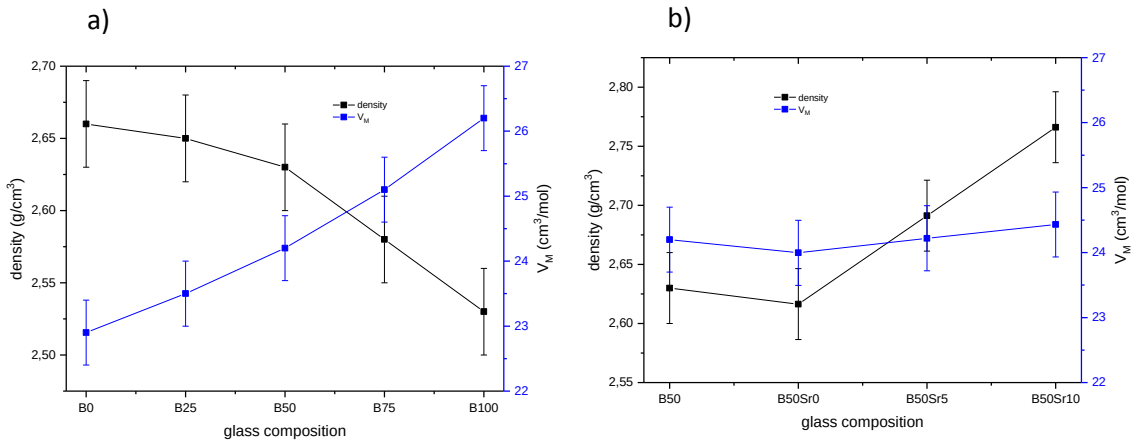

Figure 1: Density calculation for (a) borosilicate and (b) Mg/Sr substituted borosilicate bioactive glasses

The decrease in density, when substituting SiO_2 by B_2O_3 can be justified by the lower mass of boron compared to silicon. Also, an increase in the boron content, at the expense of silica, led to a decrease in the SiO_2/B_2O_3 ratio and a decrease in the Na_2O/B_2O_3 ratio. These ratios have been used in the Dell model to

discuss the structure of borosilicate glasses and are respectively labelled K and R [14]. The decreased density with increasing B_2O_3 content is also consistent with the reported data when K and/or R decreases [15, 16]. However, due to the smaller size of the boron ion compared to that of silicon, compaction of the network was expected. Instead, an expansion of the network is seen. This effect could be attributed to the formation of [BO_3] and [BO_4] units. Substitution of MgO for CaO does not influence either density or molar volume as shown in Fig. 1b. Substitution of Ca with increasing content of Sr does lead to an increase in density whereas molar volume remained unchanged. Replacement of MgO for CaO was already found to have less effect on density than SrO [17, 18].

Figure 2 presents the FTIR-ATR spectra of the glasses with various boron content.

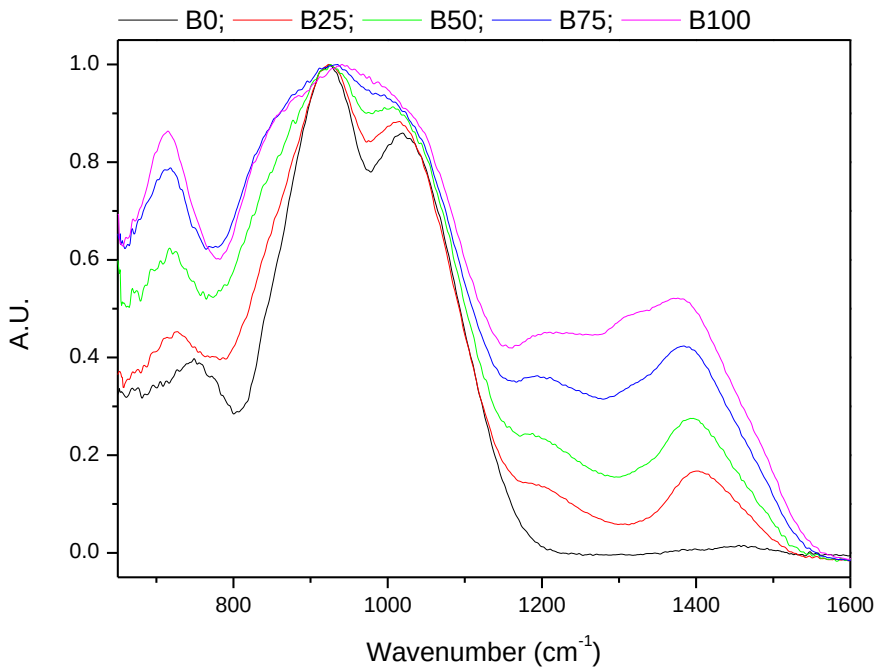

Figure 2: FTIR spectra of glasses with various B_2O_3 content.

As explained in [17], the spectrum of glass B0 shows absorption bands at 748, 1023 cm^{-1} and in the 1400–1515 cm^{-1} region. The band at 930 cm^{-1} can be attributed to $Si–O^-$ in [SiO_4] and the band peaking at 1023 cm^{-1} due to Si–O–Si asymmetric stretching in [SiO_4] units [19-21]. The band at 748 cm^{-1} is due to Si–O

bending [22]. The band located within 1400–1515 cm^{-1} is related to carbonate in the glass structure [23]. With increasing the boron content:

i) a band at 1401 cm^{-1} appears and progressively shifts to 1380 cm^{-1}. This band was attributed to the formation of [BO_3] triangles [24, 25].

ii) a shoulder at 1337 cm^{-1} and a band at 1227 cm^{-1} appeared. The shoulder was attributed to borate triangles [BO_3] and the band to [BO_2O^-] [24, 25].

iii) the two bands at 930 and 1023 cm^{-1} broadened to form one large band with full SiO_2 substitution. The broad band was attributed to a combination of vibration modes from [BO_4] units at 875 cm^{-1}, B-O-M (where M is modifying ions) in the ~992 cm^{-1} range as well as B-O-Si and B-O-B linkages [24, 25, 26]

iv) the band at 748 cm^{-1} related to Si-O bending disappeared and a new band formed at 715 cm^{-1} which grew in intensity. This new band was attributed to B-O-B bending [24, 25, 26].

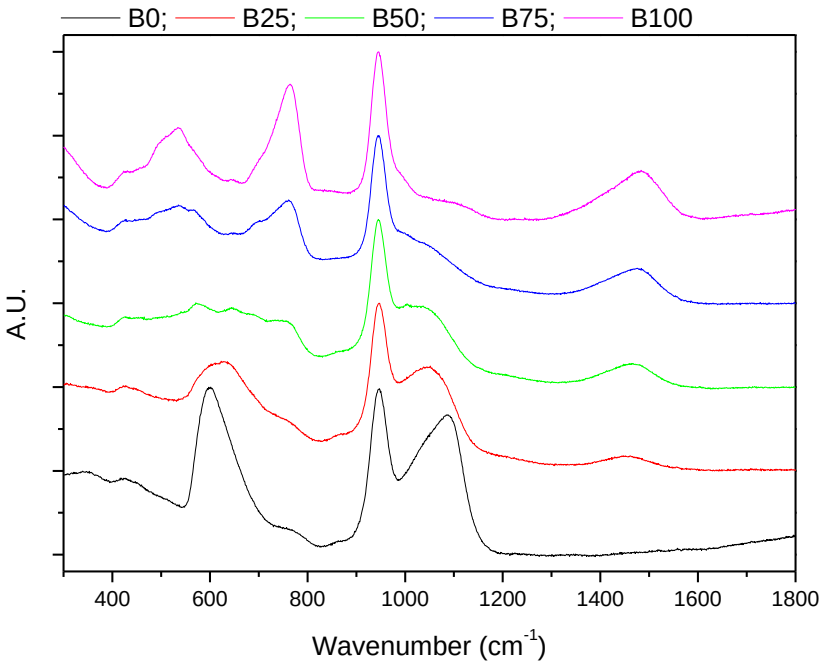

Figure 3: Raman spectra of the glasses with various B_2O_3 content.

Glass B0 (x=0) has three intense bands at 1087, 946 and 597 cm^{-1} as well as a shoulder located at 764 cm^{-1}. The band at 1087 cm^{-1} can be attributed to Si-O-Si (bridging oxygen) and Q^3 units in the silicate structure

[27, 28]. The band at 1087 cm^{-1} can be attributed to $Si\text{-}O^-$ (non-bridging oxygen) and Q^2 units [27, 28]. The band at 597 cm^{-1} corresponds to Si-O-Si rocking vibration [27]. The shoulder at 764 cm^{-1} was attributed to Si-O-Si bond bending vibration [27]. When x increases:

i) a band at ~1490 cm^{-1} appeared and grew in intensity. This band is caused by the vibration of non-bridging oxygen atoms in $B\text{Ø}_{2/2}O^-$ (where Ø corresponds to bridging oxygen) asymmetric triangles [28, 29].

ii) the band at 1087 cm^{-1} decreases in intensity and shifts to a lower wavenumber forming a shoulder (at 1000 cm^{-1}) on the spectra of B100 glass.

iii) the shoulder at 764 cm^{-1} grew in intensity and became a clear band in the B100 spectra. In borate glasses this band is often assigned to vibration of one (triborate) or two (di-triborate) tetrahedrons $[B\text{Ø}_{4/2}]^-$ [28, 30].

iv) in the 400-600 cm^{-1} region, at least three peaks formed with increasing the B_2O_3 content, at 430, 500 and 535 cm^{-1}. Peaks in this domain are often attributed to cation-oxygen bridges [31] and to B-O-Si and B-O-B bridging bonds [32, 33, 34].

With increasing SiO_2 substitution for B_2O_3, the glass structure progressively expanded as seen in Figure 1. Indeed, the boron ions are likely to form B-O-Si, diborate and non-bridging oxygens (NBOs) in the glass structure, which in turn would lead to an increase in free volume within the glass network [35].

In order to evidence the presence of $[BO_4]$ and $[BO_3]$ units as well as to better understand their conformation, NMR was conducted. The ^{11}B NMR spectra of the glasses are presented in Figure 4.

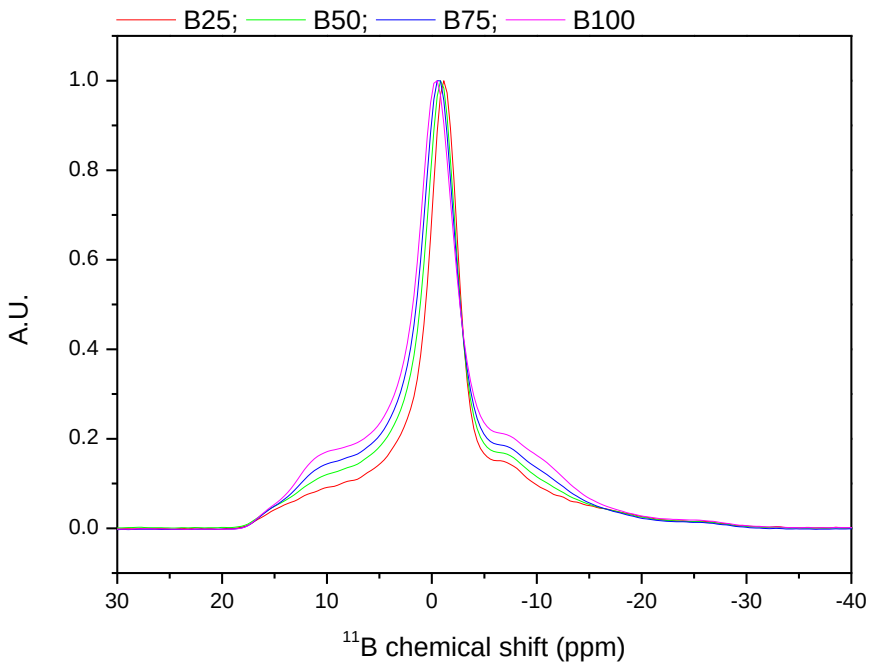

Figure 4: ^{11}B NMR spectra of the glasses with various B_2O_3 content

The major band in the 11B NMR corresponds to the $^{[4]}$B site while the broad band located around 9 ppm corresponds to the $^{[3]}$B site. Deconvolution of the NMR spectra reveals a slight increase of the proportion of $^{[3]}$B compared to the $^{[4]}$B units. Proportion of $^{[3]}$B increases from 48 to 52% with increasing boron content. The position of the $^{[3]}$B band along with presence of a band in the -7ppm region indicate the presence of planar [BO_3] rather than [BO_3] units in ring configuration as suggested by the Raman and FTIR analyses. The position of the main band, moving towards higher chemical shift, is due to the decrease in Si ions as first neighbour being progressively replaced by boron, as suggested in [36].

Replacement of Ca with Mg and/or Sr did not lead to significant structural changes.

3.2 In-vitro dissolution in simulated body fluid (SBF).

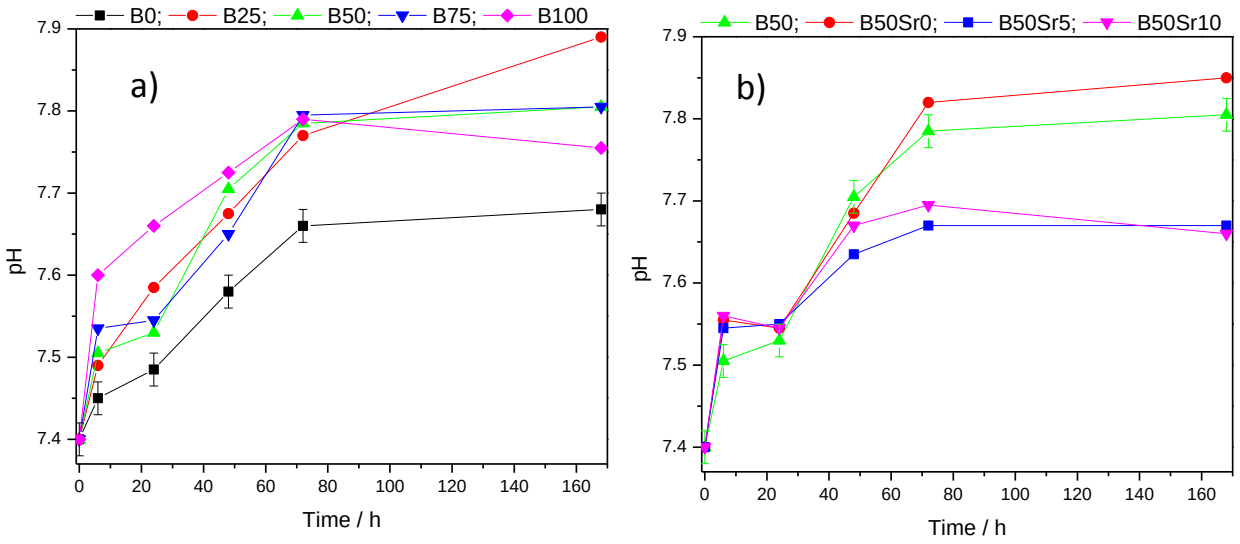

100 **Figure 5:** pH of the SBF post immersion of the investigated glasses

101

102 Figure 5 shows the change in pH in SBF as a function of immersion time for the glasses tested.

103 With increasing the immersion time, pH rises in all the solutions. All boron-containing glasses exhibit a
104 higher pH rise than the boron-free glass (Figure 5a). The rise in pH, upon immersion of bioactive silicate and
105 borosilicate glasses is due to the leaching of large amount of alkaline and alkaline earth ions in solution and
106 their subsequent substitution with hydrogen ions [37]. The initial rise in pH with increasing boron content,
107 for up to 6 hours, indicates an increased initial dissolution rate of the borosilicate compared to the silicate
108 bioactive glasses. However, the increase in the final pH is not linear with the increase in boron content in
109 the glass. Indeed, it appears that the pH show a mix glass former effect, thereby the highest pH is reported
110 for the glass with 25% SiO_2 substituted by B_2O_3. As reported elsewhere, bioactive borosilicate glasses have
111 faster dissolution kinetics and convert more completely into HA than typical silica-bioactive glasses [38, 39].
112 Therefore, the initial increase in dissolution rate is assigned to the borate sub-network which shows a
113 higher dissolution rate compared to the silica network. At longer immersion time, the maxima see for the
114 pH of the glass B25 might be due to either large boron release into solution (acidic) or to the faster
115 precipitation of a Ca/P reactive layer. From Figure 5b, substitution of MgO seems to lead to a slight increase

in pH. This might be related to the fact that, as reported by Oliveira et al. [40] MgO improves the early stages of ionic dissolution by favouring Q_0 speciation. Further substitution of CaO with SrO induces a decrease in pH. Such decrease in pH was already reported when substituting SrO for CaO in B0 glass [18].

FTIR spectra of the considered glasses before and after different soaking times in SBF are reported in Figures 6 and 7. In Figure 6, the FTIR spectra of the glasses B0, B50 and B100 at various immersion time are presented, taken as example.

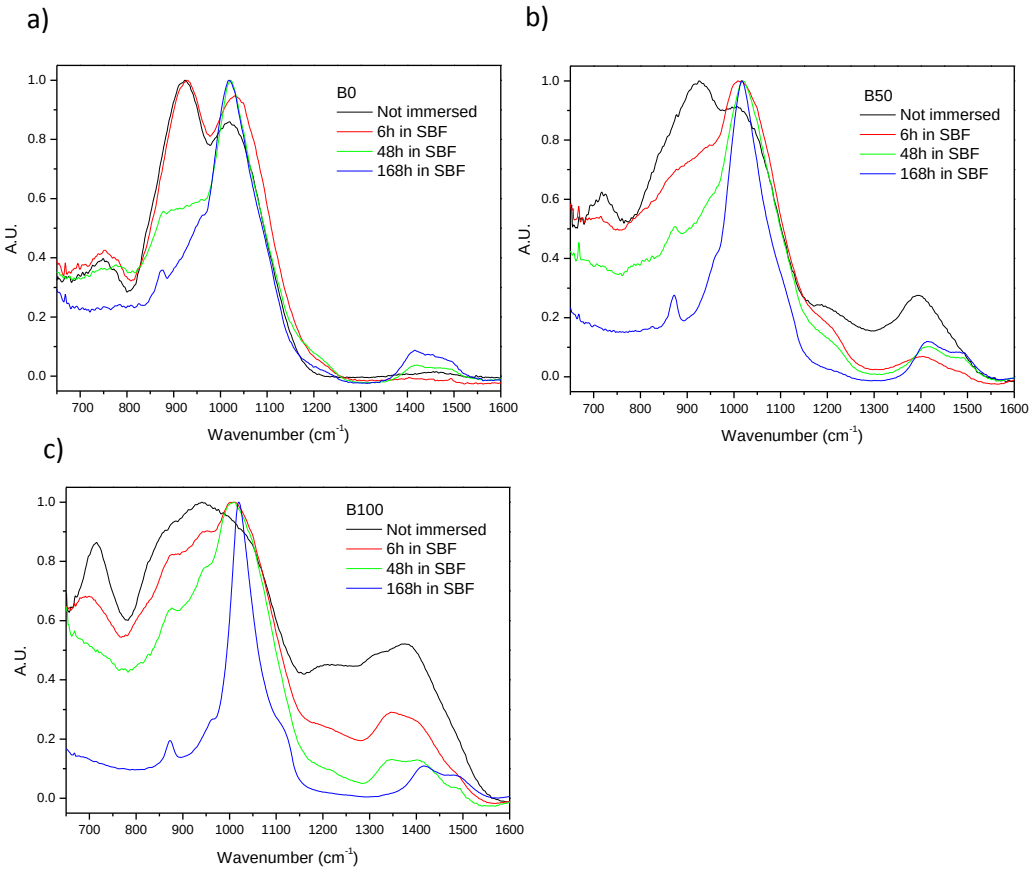

Figure 6: FTIR-ATR spectra of the glass B0 (a), B50 (b) and B100 (c) for various immersion times.

With increasing immersion time of the silicate and borosilicate glasses (Figure 6a and b), the intensities of the bands located at 748 and 930 cm^{-1} decreased. Simultaneously, the broad band at 1023 cm^{-1} increased in intensity, sharpened and shifted to higher wavenumbers. The intensity of the band related to carbonate in the 1400-1515 cm^{-1} region also increased with immersion time. A shoulder at 1212 cm^{-1} appeared after 6 h

of immersion and its intensity increased with immersion time. Lastly, a second shoulder at 875cm^{-1} appeared after one week of immersion in SBF.

In Figure 6c, it is clear that, upon immersion, the bands in the 1200-1600 cm^{-1} region, corresponding to the borate network, decreased in intensity and a doublet in the 1350-1550 cm^{-1} region appeared and increased in intensity. The broad band in the 800-1150 cm^{-1} region split into three well defined bands centered at 1009, 948 and 872 cm^{-1} after 6 hrs of immersion. For longer immersion, the band at 1009 cm^{-1} shifted to 1019 cm^{-1} while the bands at 948 and 872 cm^{-1} did not change position. The band in the low wavenumber domain completely disappeared after 48 h immersion. Figure 6b which presents the FTIR-ATR spectra of the borosilicate glass exhibits a structural change that resembles the B0 glass in the 800-1150 cm^{-1} region and the B100 in the 1200-1600 cm^{-1} region. As already discussed in [17], a decrease in the band at 930 cm^{-1}, reveals a decrease in the concentration of $Si\text{-}O^-$ and hence a decrease in [SiO_4] units. The presence of the shoulder at 959 cm^{-1} may be attributed to C-O vibration modes in CO_3^{2-} and to P-O-P bonding [41, 42]. This is further confirmed with the appearance of the shoulder at 875 cm^{-1} which can be attributed to P-O vibration [42] and the increase in the band at 1400-1515 cm^{-1} attributed to carbonate group [23]. It is clearly shown that B0 forms a hydroxycarbonated apatite (HCA) layer when immersed in SBF [43, 44]. Similarly, glasses containing boron show structural modification where the boron network is being hydrolysed and leached out into the solution with successive precipitation of HCA (Figure 6b and c). One can clearly see that the vibrations related to apatite structure are visible at earlier immersion time with increasing B_2O_3 content.

147 Figure 7 shows the FTIR spectra of the glasses B50, B50Sr0, B50Sr5 and B50Sr10 at 6h (a) and 168h (b) of
148 immersion in SBF.

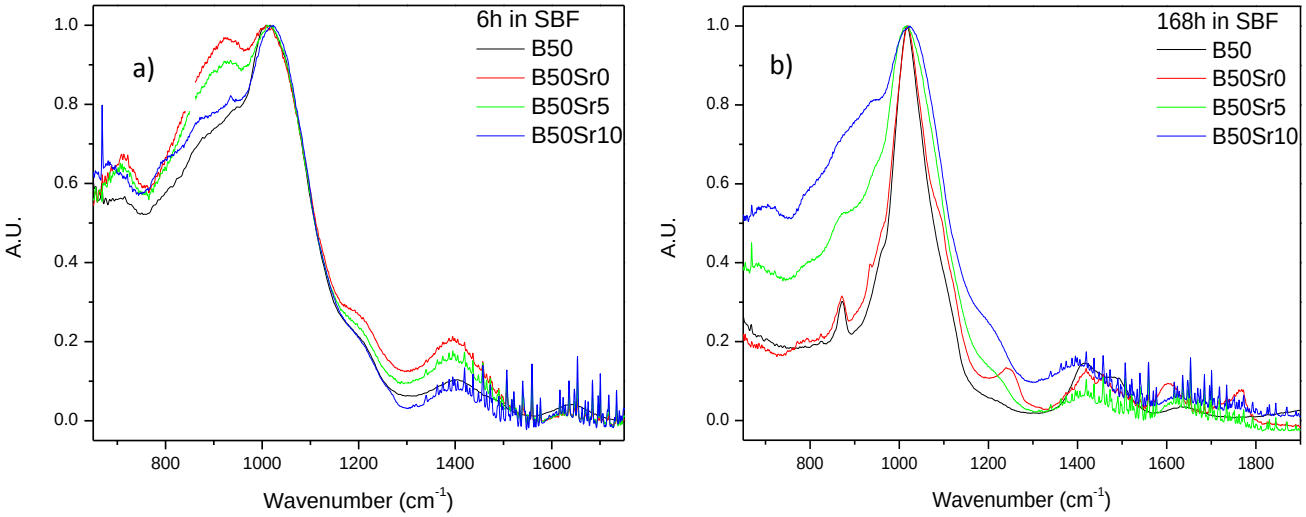

149

150 **Figure 7:** FTIR spectra of the glasses B50, B50Sr0, B50Sr5 and B50Sr10 at 6h a) and 168h b) of immersion in
151 SBF

152 As previously explained, with increasing the immersion time, the B50 glass goes through depolymerization
153 of the glass network and subsequent precipitation of a HCA layer. Addition of Mg, initially (Fig. 7a) leads to
154 a slower depolymerization of the glass network, whereas presence of SrO leads to similar surface reaction
155 as the B50 glass. At 168 h, the Mg-containing glass shows similar surface as the B50 glass, while, an increase
156 in SrO content leads to broader. This indicates that the reactive layer at the surface of the B50 and B50Sr0
157 are similar. The broader absorption bands for the strontium containing glasses indicate that precipitation of
158 the reactive layer was delayed. This is in agreement with [18] that not only discussed the delay in reactive
159 layer precipitation but also the precipitation of a Sr-substituted HAp layer.

160 The ions released in solution were quantified by ICP-OES and are presented in Figure 8. Figure 8 a) and b)
161 exhibit the silica concentration in the SBF solution for glasses with various boron content and for a
162 borosilicate glass were part of the calcium is replaced with magnesium and/or strontium, respectively.

Figure 8 c) and d) show the boron, e) and f) the phosphorous, g) and h) the calcium and i) and j) the magnesium concentration in SBF solution.

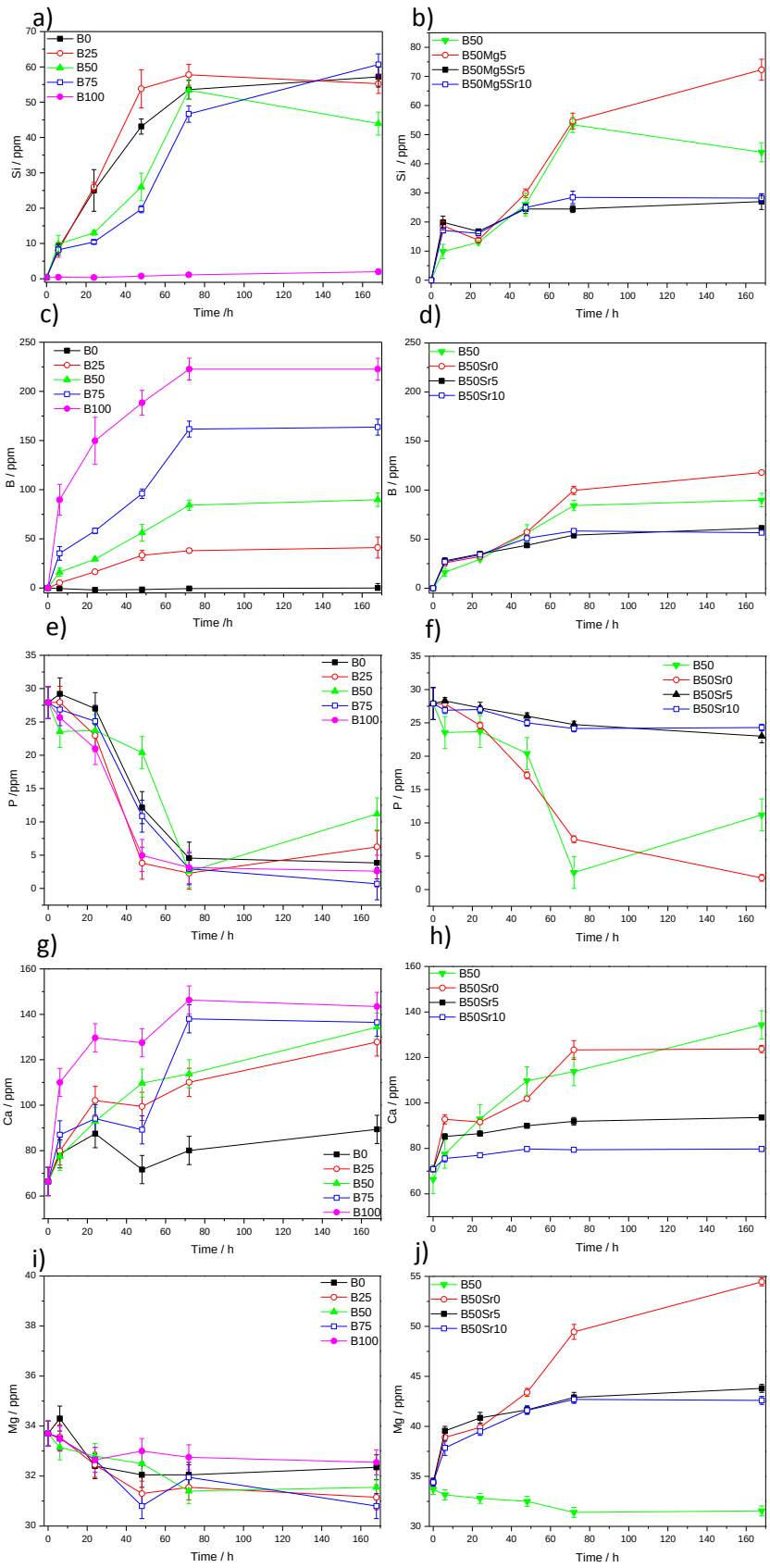

165 **Figure 8:** Si (a and b), B (c and d), P (e and (f), Ca (g and h), Mg (i and j) concentrations in SBF post

166 immersion.

Silica release (Fig. 8a), within the first 6 hours of dissolution, was comparable for all the glasses, to 8 ± 2.5 μg.ml^{-1}. A variation in the rate of release between 6 -72 hours is noticed, with B0 and B25 releasing Si faster than B50 and B75. By 72 hours, silica release was comparable for all glasses (except B75) of investigation and stabilised until the end of the study. This suggests that the soluble silica was dissolved and/or a reactive layer had precipitated, thus reducing the glass dissolution. The lower silica release at 168h for the glass B75 is believe to be due to experimental error. Furthermore, it is interesting to point out that while all the samples exhibit similar ion concentration in solution, the initial Si ions available in the glasses decreases with increasing the boron content. Therefore, almost identical ion concentration post-immersion indicates that with increasing the boron content, more of the available Silicon is being released into the solution. The boron release correlated with compositional addition, with B25 releasing the least and B100 the most (Fig. 8c). As seen with the silica release by 72 hours, the borate dissolution stabilised.

From Fig. 8e, the concentration in phosphorous decreases with increasing immersion time for all the glasses investigated. A drop in the phosphorus content is typically assigned to the precipitation of a reactive layer. B0's releases calcium initially and then the calcium concentration remained steady throughout the dissolution study, with all the values falling within 81.4 ± 7.2 μg.ml^{-1}. With increasing the boron content, an increase in the Ca concentration in the SBF, with respect to the increase in immersion time, was seen. When analysing both the change in [Ca] and [P] in tandem, it appears that the slower release of Ca for the B0 glass can be associated with the phosphorous concentration decrease. Phosphorous reduction from solution is assigned to a phosphate rich phase forming at the glass surface, for B0 this is known to be hydroxyapatite [17, 18]. From an earlier study, substitution of boron, in place of silica (in 45S5), led to an increase in the rate of precipitation of hydroxyapatite [45]. The increased release of Ca leads to faster precipitation of the reactive layer, in turn leading to a faster decrease in the phosphate content in the SBF. This suggests that full substitution of borate for silica allows greater release of cations from the glass network, due to the weaker borate bonds in contrast with silica equivalents.

Within the B0-B100 series, a decrease of magnesium was seen (Fig. 8i). This suggest that magnesium was precipitating into the calcium phosphate layer. The same conclusion has been seen within other studies for

magnesium substituted glasses [17] and it indicates that, even without addition of Mg in the based glass, part of the Mg from the SBF solution can replace Ca in the apatite structure.

Substitution of Ca with Mg, glass B50Sr0 in a borosilicate glass exhibits similar Si and B release (Fig 8b and d), for up to 48 hours of immersion. However, the Si and B concentration by 72 hours starts to deviated depending on concentration then stabilizes between 72 hours and one week. The initial P precipitation seems to be less in the Mg containing glass (Fig. 8f). Despite possessing less Ca in its composition, the initial Ca release of the Mg containing glass is initially greater. At longer immersion time, the Ca concentrations in solution are similar for both the Mg-containing and Mg free glass. Further substitution of Ca with strontium leads to a decrease in the dissolution of the glass formers, Si and B.

When increasing SrO concentration (from 5 to 10 mol%) in the glass structure did not affect the materials dissolution. The phosphate reduction and assumed precipitation was also found to be identical regardless of the SrO content in the glass. However, the phosphate reduction is less for the Sr-free glasses. The Mg release was also found to be lower for the Sr containing glass compared to the Sr-free glass. Taken together, and in correlation to the FTIR analysis, the increased Mg concentration in the SBF, due to the Mg release from the glass, clearly delayed precipitation of the reactive layer without disrupting degradation of the glass in SBF. In contrast, the presence of strontium not only delays precipitation of the reactive layer, but also delays dissolution of the glass. [18]

3.3 XPS analyses

Surface chemical composition of the considered glasses is reported in Table 2.

Despite of the absence of intentionally grafted organic molecules, a certain amount of carbon has been registered on the washed samples. This issue is not surprising for reactive materials and can be related to the adsorption of hydrocarbon contaminants from the atmosphere by the glass surfaces as well as to the surface carbonatation, as discussed in the following. No particular trends can be seen for oxygen. Si and B follow the trend expected from the theoretical compositions, except for B50Sr10, in which boron was not recorded. A decrease in the Ca content can be observed in B50Sr0 and B50Sr10 sample, according to its

partial substitution with Mg and Sr, while its increase with the B content in the washed borosilicate glasses can be associated with their increased reactivity. In fact, a decrease in the sodium content upon the washing process can be also registered, compared to the expected values, and can be attributed to its release in the washing media. Mg and Sr presence is in agreement with the theoretical composition of the glasses.

A non perfect fit of the experimental data on Si surface concentration with theoretical composition as well as certain variability on the P content (theoretically constant), especially for the B50S10 sample, can be associated with the high reactivity of the here investigated surfaces which can introduce some alteration at the surface composition compared to the bulk one. However results related specifically to surface modification appears coherent and significant, in fact the increase/appearance of Si can be evidenced upon silanization, according to the presence of this element in the APTES molecule.

The most interesting trend is within the nitrogen results, in fact, despite small contaminations on B100 and B50Sr0 washed samples, this element appears only on silanized glasses and can be associated with the presence of APTES molecules (characterized by amino groups), in accordance with previous works published by the authors [7, 46, 47]. The amount of APTES grafted is at about 2 atomic %and it is almost independent of the glass composition, as previously observed by the authors for phosphate-based glasses with different SrO content [7].

Table 2: Surface chemical composition (at%) from XPS survey analyses (w-washed, s-silanized)

	B0w	**B0s**	**B50w**	**B50s**	**B100w**	**B100s**	**B50Sr0w**	**B50Sr0s**	**B50Sr10w**	**B50Sr10s**
C	45,2	48,8	22	31,1	25,9	31	28,8	30,9	38,6	29,5
O	38,4	34,3	45,2	40,9	48,3	42,8	42,5	42,5	41,8	42
Na	11,2	7,5	6,4	7	2,4	6,5	8,7	2,7	13	3,4
Si	4	6	5,8	5,6		1,5	5,3	9,8	1,9	8,3
Ca	1,2	1,4	6,4	4,1	8,6	6,2	2,7	2,9	0,6	2,7

N		2		1,2	0,2	1,8	0,5	2,5		1,8
B			11,6	8,6	13,1	8,7	10	6,5		
P			2,7	1,3	1,5	1,6			2,8	7,5
Mg							1,2	2,1	0,6	2,9
S							0,4			
Sr									0,7	2

Looking at the high-resolution spectrum of the carbon region (Figure 9), the main contribution was represented by a signal at around284.5 eV. It can be attributed to C-C and C-H bonds and it is always present on reactive surfaces, due to the absorption of hydrocarbon contaminants from the atmosphere [47, 48, 49, 50]. On the silanized surfaces, this signal come from a combination of surface contaminants and the silane layer (C-C and C-H chains).

A contribution around 289 eV can be attributed to carbonates [51] and it is often detected on the surface of bioactive glasses due to their surface reactivity. This signal has been observed on both washed and silanized glasses, as previously observed on Bioglass substrates [46]. Conversely, the signal tends to disappear after the grafting of bigger molecules such as alkaline phosphatase or polyphenols [3, 52]

Two other signals appear on some of the samples with moderate intensity: one at about 286 eV, attributable to C-O bonds, and one around 288 eV, attributable to C=O bonds, both can be related to surface contaminations.

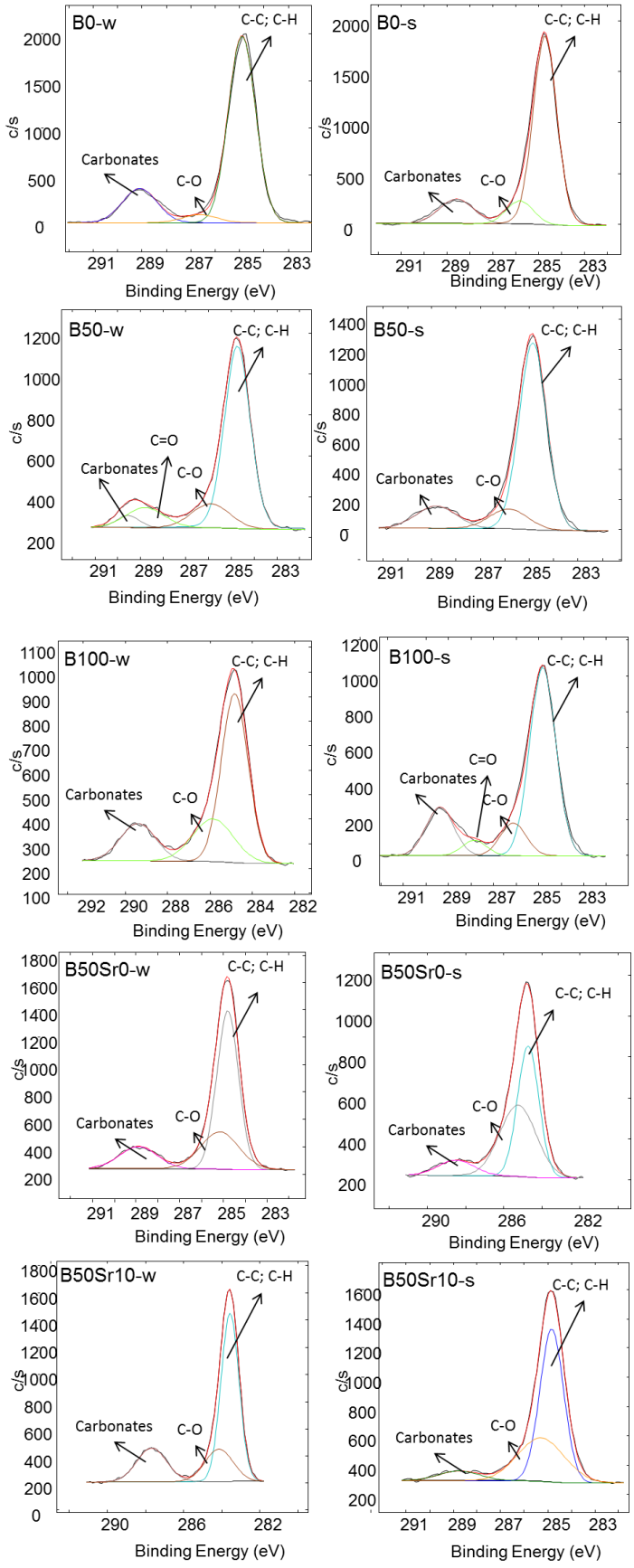

Figure 9: XPS high resolution spectra of the carbon region

The high resolution spectra of the oxygen region (not reported) confirm the hydroxylation of all the studied glasses upon washing, but no trend was observed on the basis of composition. No specific signals appeared after silanization, as expected. Since high resolution spectra of the oxygen region did not add information on the silanization ability of here investigated glasses they have not been reported and discussed in detail.

The most important data for the investigation of silanization ability of the here studied glasses resulted the high resolution spectra of the nitrogen region. They are reported, for the silanized samples (no nitrogen signals were detected on washed ones), in Figure 10 together with a schematic representation of the possible silane-surface bonding, adapted from [53, 54].

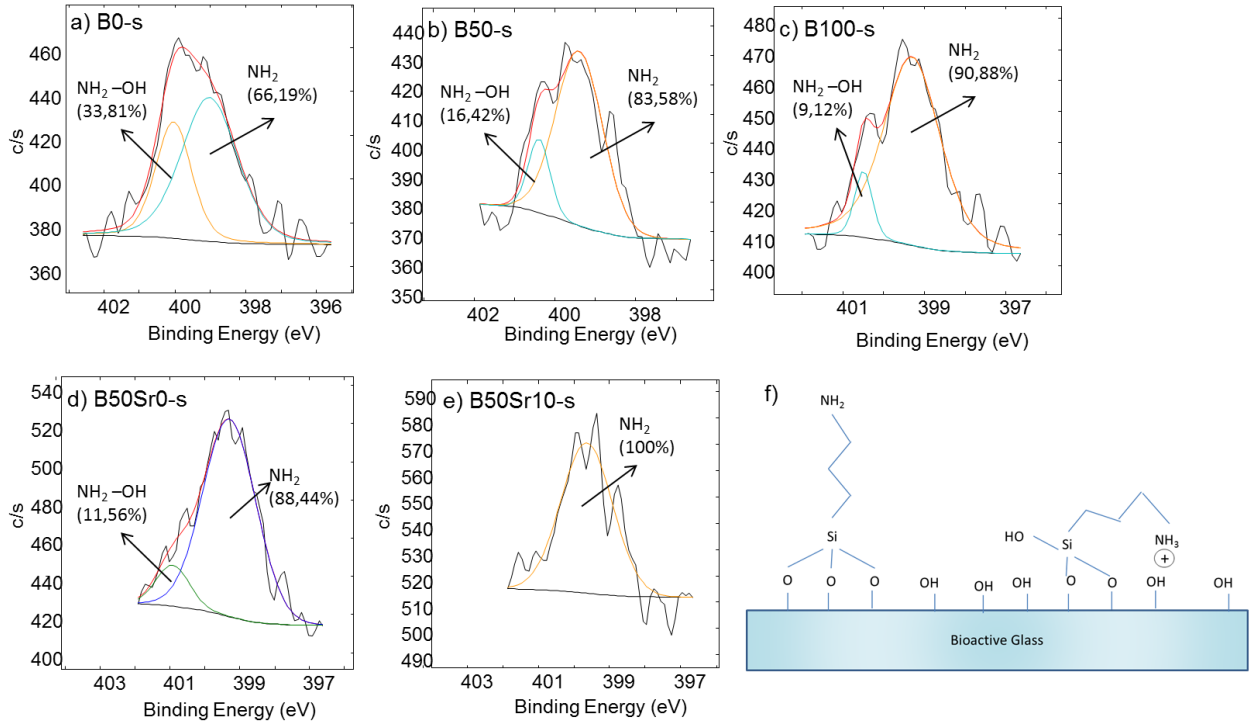

Figure 10: High resolution XPS spectra of Nitrogen region (a-e) and schematization of the silane-surface bonding

As evidenced in Figure 10f and described in [53, 54] the bonding between APTES and the glass surface can occur through the condensation of hydroxyl groups. Moreover, an interaction between silane amino groups and surface hydroxyl groups/hydroxyl groups in other silane molecules (XPS cannot discriminate between

these typologies of interaction, as discussed in [55] can be established causing the protonation of amino groups.

The high-resolution spectra of the silanized glasses evidenced two main contributions at about 399 eV and 400 eV which can be attributed to NH_2 and NH_2-OH groups respectively [47, 56-59], in accordance with the above cited binding hypothesis. An exception can be observed for B50Sr10 that has a single contribution at 399.6 eV (free amines).

An increase in the number of exposed NH_2 groups can be registered with increasing the B content in the glass from B0 to B100 (figure 10 a-c), no particular effect can be evidenced upon Mg introduction, while the complete exposition of amino groups can be obtained in the Sr containing glass. Barriers for B-O-B and B-O-Si hydrolysis are considerably lower than for Si-O-Si at neutral pH and therefore are expected to give rise to greater amount of B-OH and Si-OH group than in pure silicate glass [60].

An increase in the amine protonation has been reported for negatively charged surfaces with acidic isoelectric points [54]. Looking at zeta potential measurements (paragraph 3.6 of the present section) a trend can be observed for the borosilicate glasses, in fact the rate of free amines increases with the boron concentration in line with the isoelectric point (which moves progressively to less acidic values [61, 62]). The trend is not so clear for Mg/Sr substituted borosilicate glasses.

3.4 Contact angle measurements

As a general observation, a decrease in the water contact angle can be observed after sample washing and an increase after silanization (Figure 11), as previously observed by the authors for silica based and phosphate glasses [47-51].

The contact angle values of the polished samples do not show any specific trend, but the contact angle seems to increase with the partial substitution of B and does not seem to be influenced by Mg and Sr (Figure 11). This result can be explained considering that the behaviour of the polished samples is mainly

driven by their reactivity with atmosphere and polishing media. An increase in the contact angle with the B% can derive from the higher reactivity of B_2O_3 based glasses already evidenced in the previous sections of the present paper (Figures 5 and 8).

As evidenced in Figure 11, except for B0 (that present similar values for the contact angle before and after washing), the washed samples present a lower contact angle respect to the polished ones, as expected by the surface cleaning and exposition of OH groups. The decrement in the contact angle upon washing has maximum values for B50 and B50Sr0 samples (Figure 11).

The increase in the contact angle after APTES grafting can be ascribed to the hydrophobic nature of the bonded APTES (presence of $–NH_2$ and $–NH_3^+$ (protonated) groups together with a C-C and C-H chains) and seems to be higher for B50, B75, B50Sr0 and B50Sr5 glasses (Figure 11). This trend can be associated with an higher exposition of NH_2 groups (as suggested by XPS and zeta potential data) but further investigations are needed in order to completely clarify this point.

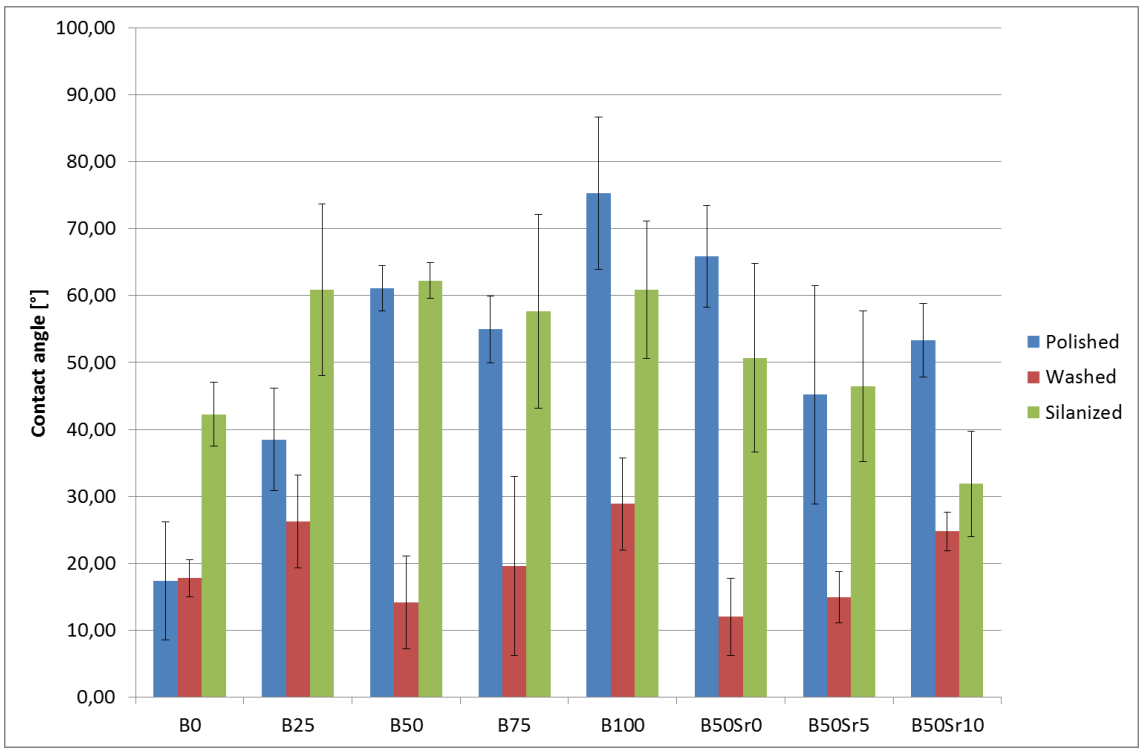

Figure 11: Contact angle measurements on polished, washed and silanized glasses

3.5 Zeta potential measurements

Zeta potential titration curves versus pH of the washed and silanized glasses are reported in figure 12. The black dots and arrows indicate the starting points of the acid and basic titrations. At the beginning of the test, the pH value of KCl electrolyte is in the 5.0-5.6 range. As it can be observed from the figure, the titration curve of B0 glass (both washed and silanized samples) starts from an unmodified pH value of the KCl solution. On the other side, an extreme situation must be evidenced for B100 glass (both the washed and silanized samples), for which strong basification occurs at the beginning of the measurement leading to a starting point of the test at pH value of 8.8. A smaller basification can be registered for B50, B50Sr0 (both washed and silanized samples) and B50Sr10 (much more evident on the silanized than on the washed sample) at the starting point of the curve. This phenomenon can be associated with the different amounts of ions released by the bioactive glasses in the electrolyte solution during the measurement setup and their surface reactivity in aqueous solutions; an increasing reactivity can be assessed moving from B0 to B50(Sr0,10) and finally to B100 on the basis of the zeta potential data. The persistence of reactivity of the B containing glasses at the very beginning of the test is in accordance with a non-continuous coating of the glass surface through silanization. In the case of B100, further considerations based on the titration curve are not reliable because, due to the strong glass reactivity, the glass surface results to be too highly modified from the very beginning of the test. Taking into account this preliminary observation, some further considerations can be made for the other materials.

Considering the measurements reported in figure 12, it can be observed that the Isoelectric Point (IEP) has been experimentally determined for B0-silanized and B50Sr0-silanized samples. In the other cases, IEP falls at too acidic values and cannot be experimentally determined [63], but it can be derived by interpolation of the titration curves.

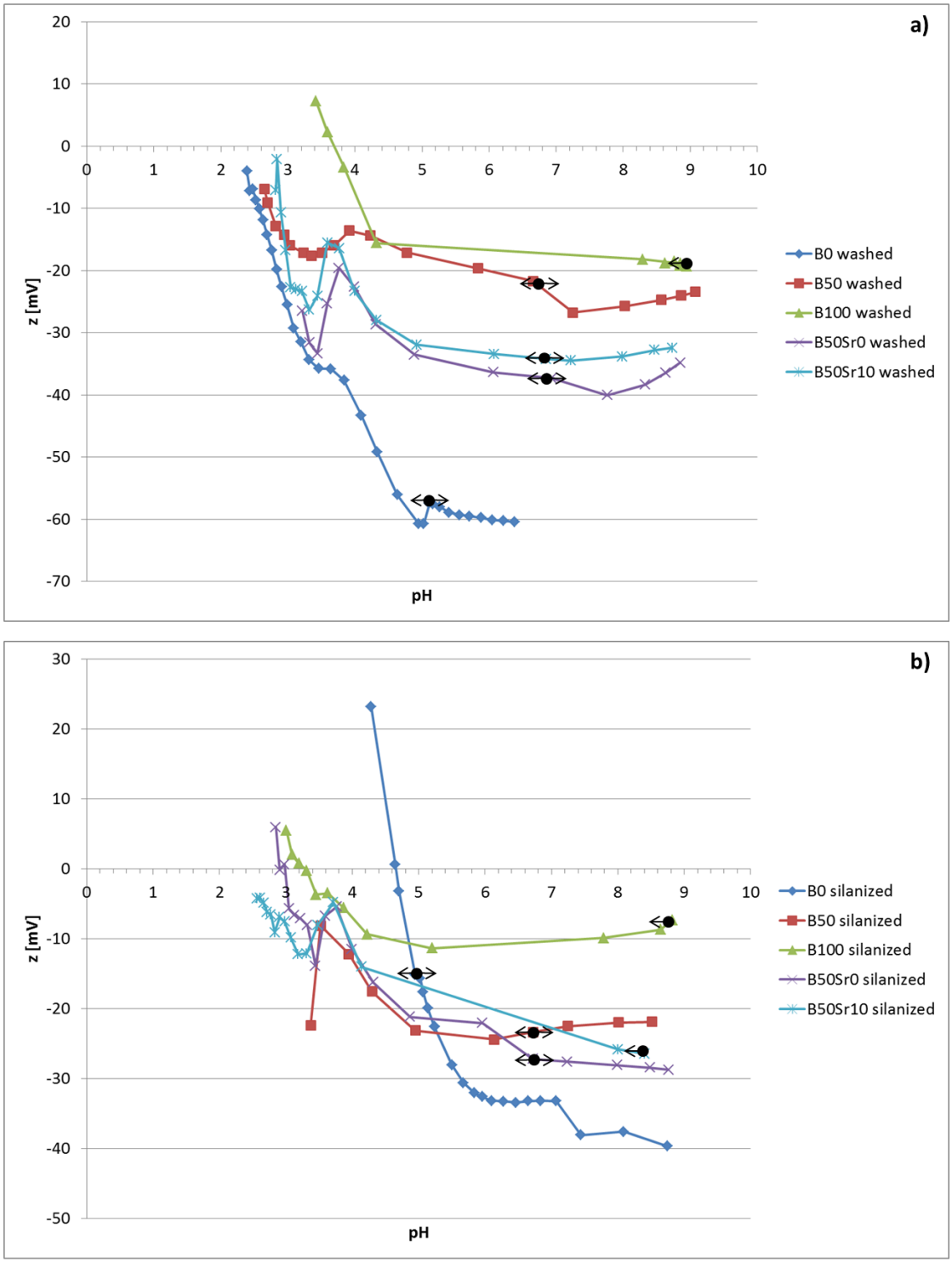

Figure 12: zeta potential vs pH for a) washed and b) silanized glasses

The isoelectric point of silica and silica based glasses is reported in literature in the pH range 2-3 [64-64] and a shift to more basic values is reported after the addition of boron in their composition [61, 62]. In

accordance with this data, a certain shift to less acidic values can be determined by interpolation with increasing the boron content in the studied glasses (washed samples).

A basic isoelectric point (9-10) is reported for APTES as well as a shift of the IEP to basic values for APTES-modified materials [59, 67, 68]. As a consequence, the APTES and APTES modified surfaces, are reported in literature to be positively charged at physiological pH [59, 67, 68]. In the case of the here investigated silanized glasses, a moderate shift of the isoelectric points to less acidic values can be observed after silanization together with a shift of the surface charge at physiological pH to less negative values. Results on B0 (the more stable glass) appear to be the most clear in this sense, in fact the IEP of washed B0 is close to 2 (from the interpolation of the titration curve in Figure 12a) while it moves to 4.65 after silanization. Moreover, the zeta potential at physiological pH (7.4) is -60mV for washed B0 while it is -38 mV for B0-sil. Despite of the cited shifts, the isoelectric point of the investigated surfaces remains in the acidic range and the charge at physiological pH is negative on all the samples. The entity of the IEP shift as well as the increase in the positive surface charge has been reported as being dependent on the density of the amino groups [68, 69]. The moderate shift observed on the here analyzed glasses can be explained considering that the proposed functionalization employs a small amount of APTES and the amount of molecules attached to the surface is relatively small (at about 2% at of N in XPS survey spectra) because it is finalized to the specific objective of functionalization. In conclusion, the zeta potential titration curves give an indication of a non-uniform coverage of the surface. Finally, a certain dissolution/detachment of the silane during the measurement (which foresees electrolyte flux on the glass surface for some hours) cannot be excluded.

A plateau in the basic region is associated with the presence of homogeneous functional groups, with acidic behavior, exposed on the surface [13]. A plateau can be observed for all the washed glasses and attributed to the exposition of hydroxyl groups upon the washing procedure. For the washed glasses, these plateaus begin at very acidic pH (at about 4) and can be correlated with a strong acidic behavior of the exposed functional groups. As far as the silanized glasses are concerned, the plateau in the basic region still persists on all the surfaces. Whereas, no plateau is visible in the acidic region on the silanized surfaces. This last

feature is observable when homogeneous exposition of functional groups with basic behavior (such as NH_2 ones) occurs and they are completely protonated at acidic pH values [13]. Actually, this condition is not reached by the analyzed silanized materials during the titration curves.

Conclusions

B0 (S53P4) bioactive glass was used as starting reference glass and progressive substitution of silica with B_2O_3 was performed up to B100 composition (fully borate glass). Partial substitution of Ca with Sr and Mg was also considered.

Both density and molar volume of the glass are influenced by the B_2O_3 substitution for SiO_2, but not by the substitution of CaO with MgO, while the substitution of CaO with SrO impacted only on the density.

Spectroscopic characterizations revealed the formation of diborate and triborate structures as well as NBO, as the B_2O_3 content increases.

Glass dissolution in TRIS and bioactivity in SBF increases for borate and borosilicate glasses with a non linear dependence on the B content. A slight decrease in apatite precipitation has been observed for sr containing glasses.

Zeta potential titration curves confirm an increasing surface reactivity of the glasses containing B in contact with aqueous solutions by increasing the B content and the presence of strong acidic OH groups on all the glasses.

3-aminopropyltryethoxysilane (APTES) was successfully grafted to all the considered glasses following a protocol previously developed by the authors for silica based and phosphate glasses, as assessed by XPS and contact angle measurements. The amount of grafted APTES is around 2%at and it is independent on the glass composition. However, this silanization protocol does not induce the formation of a continuous coating on the glass surfaces as revealed by zeta potential data.

The present research provides new information about the structure of borosilicate glasses doped with different amount of network modifying ions. An increase in surface reactivity has been observed increasing

the B content while minor impact has been induced by partial Ca substitution with Mg and Sr .Finally for the first time the present research demonstrates the possibility to effectively silanize borosilicate bioactive glasses, thus representing a promising starting point for the design of surface functionalization protocols of these class of bioactive materials with various molecules of biological interest.

References

[1] S. Ferraris and E. Verné, Chapter 9: Surface Functionalization of Bioactive Glasses: Reactive Groups, Biomolecules and Drugs on Bioactive Surfaces for Smart and Functional Biomaterials, Bioactive glasses: Fundamentals, Technology and Applications, The Royal Society of Chemistry, (eds. A.R. Boccaccini, D.S. Brauer, L. Hupa), 2017, 231-235.

[2] E. Verné,C. Vitale-Brovarone, E. Bui, C. L. Bianchi, A. R. Boccaccini, Surface functionalization of bioactive glasses, J Biomed Mater Res 90A(2009) 981–992

[3] E. Verné; S. Ferraris; C. Vitale-Brovarone; S. Spriano; .C. Bianchi; A. Naldoni; M. Morra; C. Cassinelli, Alkaline phosphatase grafting on bioactive glasses and glass-ceramics, Acta Biomater 6 (2010) 229-240

[4] SW Park, YI Kim, KH Chung, SI Hong, SW Kim. Covalent immobilization of GL-7-ACA acylase on silica gel through silanization. React Funct Polym 51 (2002) 79–92

[5] T. Tätte, K. Saal, I. Kink, A. Kurg, R. Lõhmus, U. Mäeorg, M. Rahi, A. Rinken, A. Lõhmus, Preparation of smooth siloxane surfaces for AFM visualization of immobilized biomolecules, Surf Sci 532–535 (2003) 1085–1091.

[6] X. Zhang, S. Ferraris, E. Prenesti, E. Verné, Surface functionalization of bioactive glasses with natural molecules of biological significance, part II: Grafting of polyphenols extracted from grape skin, Appl. Surf. Sci. 287 (2013) 341-348.

405 [7] J. Massera, A. Mishra, S. Guastella, S. Ferraris, E. Verné, Surface functionalization of phosphate-based
406 bioactive glasses with 3-aminopropyltriethoxysilane (APTS), Biomed. Glasses; 2 (2016) 51–62

407 [8] M. Fabert, N. Ojha, E. Erasmus, M. Hannula, M. Hokka, J. Hyttinen, J. Rocherullé, I. Sigalas, J. Massera,
408 Crystallization and sintering of borosilicate bioactive glasses for application in tissue engineering, J Mater
409 Chem B, 5 (2017) 4514-4525

410 [9] E.P. Erasmus, O.T. Johnson, I. Sigalas, J. Massera, Effects of Sintering Temperature on Crystallization and
411 Fabrication of Porous Bioactive Glass Scaffolds for Bone Regeneration, Sci Rep, 7 (2017) 6046

412 [10] W. Huang, D.E. Day, K. Kittiratanapiboon, M.N. Rahaman, Kinetics and mechanisms of the conversion
413 of silicate (45S5), borate, and borosilicate glasses to hydroxyapatite in dilute phosphate solutions, J Mater
414 Sci: Mater Med, 17 (2006) 583-596

415 [11] D. Massiot, F. Fayon, M. Capron, I. King, S. Le Calvé, B. Alonso, J.-O. Durand, B. Bujoli, Z. Gan, G.
416 Hoatson, Modelling One-Two-Dimensional Solid-State NMR Spectra, Magn Reson Chem, 40 **(**2002) 70-76.

417 [12] T. Kokubo, H. Kushitani, S. Sakka, T. Kitsugi, T. Yamamuro, Solution Able to Reproduce In Vivo Surface-
418 Structure Changes in Bioactive Glass-Ceramic A-W, J Biomed Mater Res, 24 (1990) 721-734.

419 [13] T. Luxbacher, The ZETA guide, principles of the streaming potential technique, Anton Paar.

420 [14] W.J. Dell, P.J. Bray, S.Z. Xiao, ^{11}B NMR studies and structural modeling of Na_2O-B_2O_3-SiO_2 glasses of high
421 soda content, Journal of Non-Crystalline Solids, 58 (1983) 1-16.

422 [15] J.M. Roderick, D. Holland, A.P. Howes, C.R. Scales, Density–structure relations in mixed-alkali
423 borosilicate glasses by ^{29}Si and ^{11}B MAS–NMR, J Non Cryst Solids, 293-295 (2001) 746-751.

424 [16] D. Feil, S. Feller, The density of sodium borosilicate glasses related to atomic J Non Cryst Solids, 119
425 (1990) 103-111.

426 [17] J. Massera, L. Hupa, M. Hupa, Influence of partial substitution of CaO with MgO on the thermal
427 properties and in vitro reactivity of the bioactive glass S53P4, J Non Cryst Solids 358 (2012) 2701-2707.

[18] J. Massera, L. Hupa, Influence of SrO substitution for CaO on the properties of bioactive glass S53P4, J Mater Sci Mater Med, 25 (2014) 657-668.

[19] L. Stoch, M. Sroda, Infrared spectroscopy in the investigation of oxide glasses structure, J. Mol. Struct., 511-512 (1999) 77-84

[20] M. Szumera, I. Waclawska, Z. Olenjniczak, J. Therm. Anal. Calorim., 99 (2010) 879-886.

[21] G.P. Bentrup, H.M.M. Moawad, L.F. Santos, R.M. Almeida, H. Jain, J. Am. Ceram. Soc., 92 (2009) 249-252

[22] J. Serra, P. González, S. Liste, C. Serra, S. Chiussi, B. León, M. Pérez-Amor, H.O. Ylänen, M. Hupa, FTIR and XPS Studies of Bioactive Silica Based Glasses, J Non Cryst Solids 332 (2003) 20-27.

[23] A.C. Queiroz, J.D. Santos, F.J. Monteiro, M.H. Prado da Silva, Dissolution Studies of Hydroxyapatite and Glass-Ceramic Reinforced Ceramics, Mater Charact 50 (2003) 197-202.

[24] P. Pascuta, M. Bosca, S. Rada, M. Culea, I. Bratu, E. Culea, FTIR Spectroscopic Study of Gd_2O_3-Bi_2O_3-B_2O_3 Glasses, J Optoelectron Adv M, 10 (2008) 2416-2419.

[25] L. Koudelka, P. Mosner, Borophosphate Glasses of the ZnO-B_2O_3-P_2O_5 System, Mater Lett., 42 (2000) 194

[26] C Gautam, A.K. Yadav, A.K. Singh, A Review on Infrared Spectroscopy of Borate Glasses with Effects of Different Additives, ISRN, 2012 (2012) 1-17

[27] L. Marsich, L. Moimas, V. Sergo, C. Schmid, Raman spectroscopic study of bioactive silica-based glasses: The role of the alkali/alkali earth ratio on the Non-Bridging Oxygen/Bridging Oxygen (NBO/BO) ratio, Spectroscopy, 23 (2009) 227-232.

[28] A.A. Osipov, L.M. Osipova, V.E. Eremyashev, Structure of alkali borosilicate *glasses* and melts according to Raman spectroscopy data, Glass Phys. Chem, 39 (2013) 105-112.

450 [29] T. Yano, N. Kunimine, S. Shibata, M. Yamane, Structural Investigation of Sodium Borate Glasses and
451 Melts by Raman Spectroscopy: I. Quantitative Evaluation of Structural Units, J Non Cryst Solids, 321 (2003)
452 137-146

453 [30] E.I. Kamitsos, M.A. Karakassides, Structural Studies of Binary and Pseudo Binary Sodium-Borate Glasses
454 of High Sodium Content, Phys Chem Glasses, 30 (1989) 19-26.

455 [31] D. Möncke, M. Dussauze, E.I. Kamitsos, C.P.E. Varsamis, D. Erht, Thermal poling induced structural
456 changes in sodium borosilicate glasses, Phys Chem Glasses, 50 (2009) 229-235

457 [32] O. Attos, M. Massot, M. Balkanski, E. Haro-Poniatowski, M. Asomoza, Structure of Borovanadate
458 Glasses Studied by Raman Spectroscopy, J Non Cryst Solids, 210 (1997) 163-170

459 [33] I. Ardelean, R. Lungu, P. Pascuta, Structural Changes Induced by Fe_2O_3 Addition in Strontium-Borate
460 Glass Matrix, J Mater Sci Mater Electron, 18 (2007) 837-841.

461 [34] T. Furukawa, W.B. White, Raman Spectroscopic Investigation of Sodium Borosilicate Glass Structure, J
462 Mater Sci, 16 (1981) 2689-2700.

463 [35] J.E. Shelby, Introduction to Glass Science, 2nd Edition, RSC publishing, 2005

464 [36] F. Angeli, T. Charpentier, D. de Ligny, C. Cailleteau, Boron Speciation in Soda-Lime Borosilicate Glasses
465 Containing Zirconium, J Am Ceram Soc., 93 (2010) 2693-2704.

466 [37] L.L. Hench, D.E. Day, W. Höland, V.M. Rheinberger, Glass and Medicine, Int. J. Appl. Glass Sci, 1 (2010)
467 104-117

468 [38] R.F. Brown, M.N. Rahaman, A.B. Dwilewicz, W. Huang, D.E. Day, Y. Li, B.S. Bal, Effect of Borate Glass
469 Composition on its Conversion to Hydroxyapatite and on the Proliferation of MC3T3-E1 Cells, J Biomed
470 Mater Res A, 88A (2009) 392-400

471 [39] S.B. Jung, D.E. Day, Conversion kinetics of silicate, borosilicate, and borate bioactive glasses to
472 hydroxyapatite, Phys Chem Glasses B, 50 (2009) 85-88.

473 [40] J.M. Oliveira, R.N. Correia, M.H. Fernandes, Effects of Si speciation on the in vitro bioactivity of glasses,
474 Biomaterials 23 (2002) 371–379

475 [41] E. Saiz, M. Goldman, J.M. Gomez-Vega, A.P. Tomsia, G.W. Marshall, S.J. Marshall, In vitro behavior of
476 silicate glass coatings on Ti6Al4V, Biomaterials, **23** (2002) 3749-3756.

477 [42] I. Rehman, J.C. Knowles, W. Bonfield, Analysis of in vitro reaction layers formed on Bioglass® using thin-
478 film X-ray diffraction and ATR-FTIR microspectroscopy, J Biomed Mater Res, **41** (1998) 162-166.

479 [43] Ö.H. Andersson, K.H. Karlsson, K. Kangasniemi, Calcium phosphate formation at the surface of
480 bioactive glass in vivo, J Non Cryst Solids, **119** (1990) 290–296.

481 [44] Ö.H. Andersson, I. Kangasniemi, Calcium phosphate formation at the surface of bioactive glass in vitro,
482 J Biomed Mater Res, **24** (1991) 1019–1030.

483 [45] W. Huang, D.E. Day, K. Kittiratanapiboon, M.N. Rahaman, Kinetics and mechanisms of the conversion
484 of silicate (45S5), borate, and borosilicate glasses to hydroxyapatite in dilute phosphate solutions, J. Mater.
485 Sci. Mater. Med., 17 (2006) 583-596

486 [46] E. Vernè, S. Ferraris, C. Cassinelli, A.R. Boccaccini, Surface functionalization of Bioglass® with alkaline
487 phosphatase, Surf Coat Tech 264 (2015) 132–139

488 [47] S. Ferraris, S. Perero, E. Vernè, E. Battistella, L. Rimondini, M. Ferraris, Surfacefunctionalization of Ag–
489 nanoclusters–silica composite films for biosensing, Mater. Chem. Phys. 130 (2011) 1307–1316.

490 [48] M. Textor, C. Sittig, V. Frauchiger, S. Tosetti, D.M. Brunette, Properties and bio-logical significance of
491 natural oxide films on titanium and its alloys, in: P.Tengvall, M. Textor, P. Thomsen (Eds.), Titanium in
492 Medicine, Springer-Verlag,Berlin, Heidelberg, New York, 2001, pp. 171–230.

493 [49] M. Morra, C. Cassinelli, G. Buzzone, A. Carpi, G. DiSanti, R. Giardino, M. Fini, Sur-face chemistry effects
494 of topographic modification of titanium dental implantsurfaces, 1 surface analysis, Int. J. Oral Maxillofac.
495 Implants 18 (2003) 40–45.

496 [50] M.P. Ferraz, F.J. Monteiro, J.D. Santos, CaO–P2O5glass hydroxyapatite doublelayer plasma spray
497 coating: in vitro bioactivity evaluation, J. Biomed. Mater.Res. 45 (1999) 376–383.

498 [51] X-Ray Photoelectron Spectroscopy Reference pages, 2013, C1s
499 Carbonates:http://www.xpsfitting.com/2011/03/c-1s-carbonates.html, Copyright M.C.Biesinger
500 (http://www.xpsfitting.com/), (8 May 2013, 11:14 am).

501 [52] X. Zhang, S. Ferraris, E. Prenesti, E. Verné Surface functionalization of bioactive glasses with natural
502 moleculesof biological significance, Part I: Gallic acid as model molecule, Appl Surf Sci 287 (2013) 329– 340

503 [53] Russo L, Taraballi F, Lupo C, Poveda A, Jimenez-Barbero J, Sandri M, Tampieri A, Nicotra F, Cipolla L:
504 “Carbonate hydroxyapatite functionalization: a comparative study towards (bio)molecules fixation”,
505 Interface Focus 4: 20130040. http://dx.doi.org/10.1098/rsfs.2013.0040

506 [54] Z. Xu, Q. Liu, JA Finch, Silanation and stability of 3-aminopropyl triethoxy silane on nanosized
507 superparamagnetic particles: I. Direct silanation, Appl Surf Sci 120 (1997) 269-278

508 [55] E. Metwalli, D. Haines, O. Becker, S. Conzone, CG Pantano, Surface characterization of mono-, di-, and
509 tri-aminosilane treated glass substrate, Journal of Colloid and interface science 298 (2006) 825-831

510 [56] Mohapatra S., Mallick S.K., Maiti T.K., Ghosh S.K., Pramanik P., “Synthesis of highly stable folic acid
511 conjugated magnetite nanoparticles for targeting cancer cells”, Nanotechnology 18 (2007), 385102.

512 [57] Das M., Mishra D., Maiti T.K., Basak A., Pramanik P., Biofunctionalization of magnetite nanoparticles
513 using an aminophosphonic acid coupling agent: new, ultradispersed,iron-oxide folate nanoconjugates for
514 cancer-specific targeting, Nanotechnology 19 (2008), 415101

515 [58] Y Zhang, Y Yuan, C Liu, Fluorescent labeling of nanometer hydroxyapatite, J Mater Sci Tech, 24 (2008)
516 187

517 [59] Z. Xu, Q. Liu, JA Finch, Silanation and stability of 3-aminopropyl triethoxy silane on nanosized
518 superparamagnetic particles: I. Direct silanation, Appl Surf Sci 120 (1997) 269-278

519 [60] P. Zapol, H. He, K. D. Kwon, L.J. Criscenti, First-Principles Study of Hydrolysis Reaction Barriers in a
520 Sodium Borosilicate Glass, Int. J. of Appl. Glass Sci., 4 (2013) 395-407.

521 [61] J. Blass, O. Kohler, M. Fingerle, C. Muller, C. Ziegler, Propertioes and characteristics of wet (HF) and dry
522 (RIE) etched borosilicate glass, Phys Status Solidi A 210 (2013) 988-993

523 [62] MJ Owen, PR Dvornic, Silicone Surface Science, Springler

524 [63] M. Cazzola, I Corazzari, E. Prenesti, E. Bertone, E. Vernè, S. Ferraris, Bioactive glass coupling with
525 natural polyphenols: surface modification, bioactivity and anti-oxydant ability, Appl Surf Sci 367 (2016) 237-
526 248 (s26)

527 [64] M. Kosmulsky, pH-dependent surface charging and points of zero charge. IV. Update and new
528 approach Colloid Interface Sci. 337 (2009) 439-448

529 [65] M. Cazzola, I Corazzari, E. Prenesti, E. Bertone, E. Vernè, S. Ferraris, Bioactive glass coupling with
530 natural polyphenols: surface modification, bioactivity and anti-oxydant ability, Appl Surf Sci 367 (2016) 237-
531 248

532 [66] S. Spriano, V. Sarath Chandra, A. Cochis, F. Uberti, L. Rimondini, E. Bertone, A. Vitale, C. Scolaro, M.
533 Ferrari, F. Cirisano, G.Gautier di Confiengo, S. Ferraris, How do wettability, zeta potential and hydroxylation
534 degree affect the biological response of biomaterials?, Mat Sci Eng C 74 (2017) 542–555

535 [67] Z. Wu, H. Xiang, T. Kim, MS Chun, K Lee, Surface properties of submicrometer silica spheres modified
536 with aminopropyltriethoxysilane and phenyltriethoxysilane, J Colloid Interface Sci. 304 (2006) 119-124

537 [68] RA Bini, RFC Marques, FJ Santos, JA Chaker, M Jafelici Jr, Synthesis and functionalization of magnetite
538 nanoparticles with different amino-functional alkoxysilanes, J Magn Magn Mater. 324 (2012) 534-539

539 [69] S. Campelj, D. Makovec, M. Drofenik, Functionalization of magnetic nanoparticles with 3-aminopropyl
540 silane, Journal of Magnetism and Magnetic Materails 321 (2009) 1346-1350

541